Intracisternal *Gtf2i* Gene Therapy Ameliorates Deficits in Cognition and Synaptic Plasticity of a Mouse Model of Williams–Beuren Syndrome

Cristina Borralleras[1,2,3], Ignasi Sahun[4], Luis A Pérez-Jurado[1,2,3] and Victoria Campuzano[1,2,3]

[1]Neurosciences Program, Institut Hospital del Mar d'Investigacions Mèdiques (IMIM), Unitat de Genètica, Barcelona, Spain; [2]Departament de Ciències Experimentals i de la Salut, Universitat Pompeu Fabra, Barcelona, Spain; [3]Centro de Investigación Biomédica en Red de Enfermedades Raras (CIBERER), ISCIII, Spain; [4]PCB-PRBB Animal Facility Alliance, Barcelona, Spain

Williams–Beuren syndrome (WBS) is a neurodevelopmental disorder caused by a heterozygous deletion of 26–28 genes at chromosome band 7q11.23. Haploinsufficiency at *GTF2I* has been shown to play a major role in the neurobehavioral phenotype. By characterizing the neuronal architecture in four animal models with intragenic, partial, and complete deletions of the WBS critical interval (*ΔGtf2i*$^{+/-}$, *ΔGtf2i*$^{-/-}$, PD, and CD), we clarify the involvement of *Gtf2i* in neurocognitive features. All mutant mice showed hypersociability, impaired motor learning and coordination, and altered anxiety-like behavior. Dendritic length was decreased in the CA1 of *ΔGtf2i*$^{+/-}$, *ΔGtf2i*$^{-/-}$, and CD mice. Spine density was reduced, and spines were shorter in *ΔGtf2i*$^{-/-}$, PD, and CD mice. Overexpression of *Pik3r1* and downregulation of *Bdnf* were observed in *ΔGtf2i*$^{+/-}$, PD, and CD mice. Intracisternal *Gtf2i*-gene therapy in CD mice using adeno-associated virus resulted in increased m*Gtf2i* expression and normalization of *Bdnf* levels, along with beneficial effects in motor coordination, sociability, and anxiety, despite no significant changes in neuronal architecture. Our findings further indicate that *Gtf2i* haploinsufficiency plays an important role in the neurodevelopmental and cognitive abnormalities of WBS and that it is possible to rescue part of this neurocognitive phenotype by restoring *Gtf2i* expression levels in specific brain areas.

Received 13 April 2015; accepted 12 July 2015; advance online publication 8 September 2015. doi:10.1038/mt.2015.130

INTRODUCTION

Williams–Beuren Syndrome (WBS; OMIM 194050) is a rare neurodevelopmental disorder caused by a heterozygous deletion of 26–28 contiguous genes on chromosome band 7q11.23.[1,2] It usually occurs sporadically with an incidence of 1/7,500 newborns.[3] In addition to characteristic physical features and medical problems mainly affecting the cardiovascular, endocrine, and connective tissues, WBS patients display a characteristic cognitive and behavioral profile including intellectual disability, anxiety and phobias, overfriendly personality, and visuospatial construction deficits.[4,5]

Neurologic examination and brain imaging in WBS patients have shown changes in brain anatomy and function, including significant reductions in total brain volume, being white matter more reduced than gray matter.[6–10] Structural alterations have been found in different brain regions such as amygdala, brain stem, cerebellum, corpus callosum, hippocampus, and thalamus,[6–8,11–13] as well as abnormalities of cortical surface folding patterns.[9,14,15] Functional brain alterations in the orbitofrontal cortex and visual system have also been reported using functional magnetic resonance imaging.[16–18] Depression of hippocampal energy metabolism and synaptic activity by multimodal neuroimaging also indicated an abnormal functionality of hippocampus in WBS.[11] Altered brain structure has also been reported in different WBS mouse models.[19–24] Male mice with deletion of the proximal interval (PD) had normal brain size with a strikingly reduced lateral ventricle and a significantly increased neuronal density restricted to layer V of the somatosensory cortex.[21] On the other hand, male mice with the complete deletion (CD) showed a global reduction in brain weight, with a significant volume reduction of the hippocampus and a general decrease in the cellular density of the amygdala.[19]

Clinical–molecular correlations in patients with atypical 7q11.23 deletions suggested that hemizygosity of the GTF2I family of transcription factors (*GTF2I* and *GTF2IRD1*) is the major contributor to the craniofacial features and several aspects of the neurocognitive profile such as intellectual disability, visuospatial construction deficits, and sociability.[25–29] Studies in mice have also strengthened the idea that *Gtf2i* is one of the main players in motor coordination, locomotor activity, anxiety behavior, sound intolerance, hypersociability, and craniofacial features.[20,21,30]

In order to further demonstrate the implication of *GTF2I* and better understand the pathophysiologic mechanisms underlying the neurocognitive profile of WBS, we have compared the neurobehavioral phenotype and further characterized the neuronal architecture in several mouse models of the disorder with single-gene (*Gtf2i*), partial and complete deletions of the critical interval. We then attempted a phenotypic rescue by *in situ*

Correspondence: Victoria Campuzano, Neurosciences Program, IMIM - Institut Hospital del Mar d'Investigacions Mèdiques, Unitat de Genètica, 08003 Barcelona, Spain. E-mail: victoria.campuzano@upf.edu

delivery (intracisternal) of recombinant adeno-associated viruses (AAV)-based *Gtf2i* gene therapy in adult CD mice. AAV are non-integrative viruses that are able to sustain a long-term transgene expression and to transduce both dividing and nondividing cells with low secondary effects due to their lack of pathogenicity, poor immunogenicity, and an excellent safety profile.[31–34] Here, we present evidence that *Gtf2i* haploinsufficiency is a major player in some neuroanatomical, synaptic plasticity, and cognitive alterations observed in WBS mutant mice and that the increase of *Gtf2i* expression by gene therapy is able to improve cognition and synaptic plasticity in mice with the complete deletion of the WBS genetic interval.

RESULTS

Altered neuronal architecture and impaired synaptic plasticity marker expression in the hippocampus of WBS mouse models

Little is known about neural architecture in WBS patients and mouse models. We previously reported preliminary analyses of the CA1 hippocampal morphology of CD mice suggesting a reduction in both dendritic length and spine density of apical dendrites.[19] We further studied dendritic morphology in hippocampus of all mouse models. Dendritic length was significantly different among genotypes in both, stratum radiatum (SR) ($F_{4,551}$ = 37.974; $P = 4.47 \times 10^{-28}$) and stratum oriens (SO) ($F_{4,551}$ = 31.518; $P = 1.16 \times 10^{-23}$). Dendritic length (SR and SO) was shorter in *ΔGtf2i*$^{+/-}$ (13–17%), *ΔGtf2i* $^{-/-}$ (15–16%), and CD (12–16%) mice (**Figure 1a**). Spine density on apical proximal dendrites of CA1 pyramidal neurons was reduced by 14, 15, and 17% in *ΔGtf2i* $^{-/-}$ (P = 0.003), PD (P = 0.002), and CD ($P = 2 \times 10^{-5}$), respectively (**Figure 1b** and **Supplementary Figure S1a**). Spine length was significantly reduced in all mutant mice ($F_{4,1534}$ = 17.083; $P = 1.02 \times 10^{-13}$), by 13, 15, 9, and 19% in *ΔGtf2i*$^{+/-}$, *ΔGtf2i*$^{-/-}$, PD, and CD, respectively (**Figure 1c**). No differences in spine density or mean spine length were found on basal proximal dendrites of CA1 pyramidal neurons respect to wild type (WT; **Supplementary Figure S1b,c**). All these features suggest a role of *Gtf2i* in hippocampal neural morphology.

Brain-derived neurotrophic factor (BDNF) plays an important role in the development, trophic support, synaptic transmission, and neural plasticity of the hippocampus.[35–38] In neurons, BDNF activates several intracellular pathways such as PI3K–Akt–mTOR and the Ras–ERK signaling pathways, which in turn regulate dendritic branching, dendrite size, as well as the

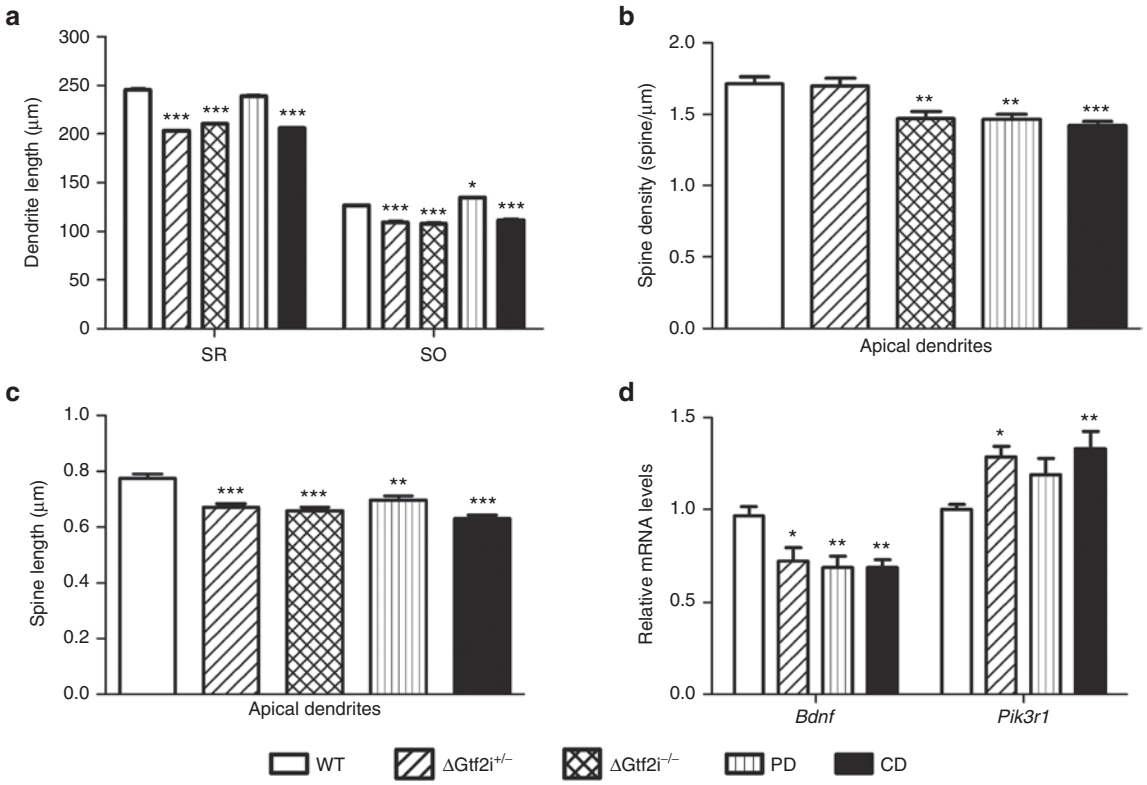

Figure 1 Neuronal architecture in CA1 pyramidal neurons and synaptic plasticity markers quantification in WBS mouse models. (**a**) Width of SR (length of apical dendrites) and SO (length of basal dendrites) was measured in CA1 area of hippocampus. Apical and basal dendrites were significantly shorter in *ΔGtf2i*$^{+/-}$, *ΔGtf2i*$^{-/-}$, and CD with respect to WT ($P < 0.001$ in all cases). PD mice had significantly longer basal dendrites (P = 0.039) than WT mice (n = 25–32 neurons/mice, ≥3 mice). (**b**) Spine density on apical proximal dendrites was significantly different among genotypes ($F_{4,149}$ = 10.644; $P = 1.29 \times 10^{-7}$; n = 8–16 dendrites/mice, ≥3 mice). (**c**) Spine length on apical proximal dendrites was reduced by 13, 15, 9, and 19% in *ΔGtf2i*$^{+/-}$, *ΔGtf2i*$^{-/-}$, PD, and CD, respectively ($F_{4,1534}$ = 17.083; $P = 1.02 \times 10^{-13}$; n = 100 spines/mice, ≥3 mice). (**d**) Hippocampal basal levels of *Bdnf* and *Pik3r1* were measured in WBS mutant mice. *Bdnf* was significantly decreased in all WBS mutant mice with respect to WT ($F_{3,40}$ = 6.476; P = 0.001). *Pik3r1* was increased in all mutant mice ($F_{3,40}$ = 5.209; P = 0.003; n = 2–4 RT-PCRs/mice, ≥4 mice). Data are presented as the mean ± SEM. P values are shown with asterisks indicating values that are significantly different in group comparisons (one-way analysis of variance followed by Bonferroni *post hoc* test). *$P < 0.05$; **$P < 0.01$; ***$P < 0.001$.

number and morphology of dendritic spines.[39–41] Interestingly, chromatin immunoprecipitation studies demonstrated that *Pik3r1*, which encodes the 85 kDa regulatory subunit of PI3K, is a direct target of GTF2I.[42] We therefore studied *Bdnf* and *Pik3r1* mRNA levels in the hippocampus of mutant and WT mice, as possible markers of synaptic plasticity. *ΔGtf2i*$^{+/-}$, PD, and CD mice had significantly lower levels of *Bdnf* mRNA (P = 0.020, P = 0.006, and P = 0.004, respectively; **Figure 1d**). Moreover, *ΔGtf2i*$^{+/-}$ and CD mice had significantly higher levels of *Pik3r1* (P = 0.042 and P = 0.004, respectively). In PD mice, *Pik3r1* expression was slightly higher although not reaching statistical significance (P = 0.274; **Figure 1d**).

Altered cognitive behavior in WBS mouse models

People with WBS are hypersociable from early in life, including an overfriendly attitude toward strangers.[43] In previous reports, the heterozygous *Gtf2i* knockout as well as CD mice showed increased social interaction and retained social interest to repeated stimuli when compared to WT mice.[19,30] PD mice also showed altered social behavior in four different sociability tests.[21] We performed a direct social test comparing the behavior of all exposed animals. *ΔGtf2i*$^{+/-}$, *ΔGtf2i*$^{-/-}$, and CD mice spent more time sniffing the container with the intruder mouse rather than the empty one (P = 0.006, P = 0.004, and P = 7 x 10^{-5}, respectively; **Figure 2a**), indicating an enhanced sociability in these animals.

Poor balance and coordination have been reported in WBS patients.[4,44] Motor coordination, as assessed by the rotarod test, was also found impaired in CD and PD mice. These results obtained with the rotarod test suggested that the proximal genes deleted in PD mice are the ones significantly contributing to this phenotype in WBS.[19,21] We performed the accelerating rotarod to test motor coordination and motor skill learning in *ΔGtf2i*$^{+/-}$ and *ΔGtf2i*$^{-/-}$ mice. Both mutant mice performed worse in the rod as early as 10 rpm ($F_{2,28}$ = 4.311; P = 0.024; **Figure 2b**). Additionally, *ΔGtf2i*$^{-/-}$ mice required a significantly larger number of trials to learn the test (P = 0.0006; **Supplementary Figure S2**). These results indicate that *Gtf2i* could be a major player in this particular phenotype. In agreement with our previous results, CD mice fell off the rod as soon as 7 rpm (P = 0.004; **Figure 2c**).

More than 80% of WBS adult individuals have anxiety, preoccupations, or obsessions.[4] In several mouse models of WBS, different paradigms evaluating anxiety have been used with controversial results.[19–21] Despite the controversial use of marble burying test as a model of anxiety or obsessive–compulsive traits,[45–47] we decided to use this paradigm because it is believed to partially depend on hippocampal function.[48,49] *ΔGtf2i*$^{-/-}$ and PD mice

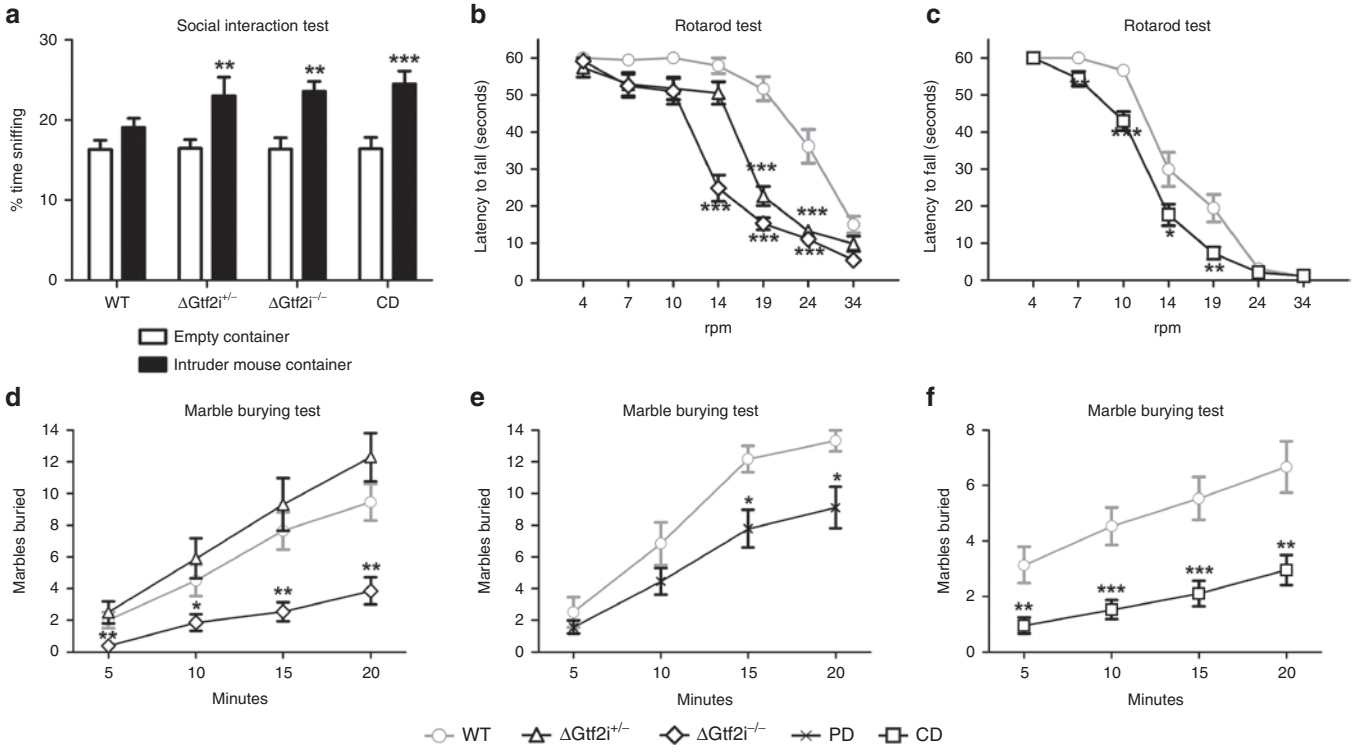

Figure 2 Cognitive behavior in WBS mouse models. (**a**) In the direct social test, *ΔGtf2i*$^{+/-}$, *ΔGtf2i*$^{-/-}$, and CD mice spent significantly (P = 0.006, P = 0.004, and P = 7 x 10^{-5}) more time sniffing the container with the intruder mouse rather than the empty container (n = 15 WT, n = 12 *ΔGtf2i*$^{+/-}$, n = 11 *ΔGtf2i*$^{-/-}$, and n = 18 CD). (**b,c**) Motor coordination and balance were assessed in the accelerating rotarod test. *ΔGtf2i*$^{+/-}$ and *ΔGtf2i*$^{-/-}$ mice had motor coordination and balance impairment as soon as 10 rpm (($F_{2,26}$ = 4.311; P = 0.024); n = 12 WT, n = 12 *ΔGtf2i*$^{+/-}$, n = 12 *ΔGtf2i*$^{-/-}$). CD mice fell off the rod as soon as 7 rpm (P = 0.004; n = 15 WT and n = 17 CD). (**d–f**) Anxiety-like/obsessive behavior was assessed in the marble burying test. The number of buried marbles (>2/3 marble covered) was counted every 5 minutes during 20 minutes. *ΔGtf2i*$^{-/-}$, PD, and CD mice showed reduced burying of marbles ($F_{1,27}$ = 12,684; P = 0.001, $F_{1,13}$ = 6.017; P = 0.029, and $F_{1,32}$ = 16.629; P<0.001, respectively; n = 6–16 WT, n = 10 *ΔGtf2i*$^{+/-}$, n = 13 *ΔGtf2*$^{-/-}$, n = 9 PD, and n = 19 CD). Circles, WT; triangles, *ΔGtf2i*$^{+/-}$; diamonds, *ΔGtf2i*$^{-/-}$; blades, PD; and squares, CD. Data are presented as the mean ± SEM. P values are shown with asterisks indicating values that are significantly different in individual group comparisons (General Linear Models of repeated measures analysis of variance, one way analysis of variance followed by Bonferroni *post hoc* test or Mann–Whitney U-test). *P < 0.05; **P < 0.01; ***P < 0.001.

showed significant reduced burying of marbles ($F_{1,27}$ = 12.684; P < 0.001 and $F_{1,13}$ = 6.017; P = 0.029, respectively; **Figure 2d,e**), pointing to abnormal levels of anxiety-like/obsessive behavior in these mice due in part to *Gtf2i* expression levels. As expected, CD mice also showed the same abnormal behavioral pattern in basal conditions ($F_{1,32}$ = 16.62874; P < 0.001; **Figure 2f**).

Efficient AAV9-mediated *Gtf2i* expression in mouse hippocampus

We generated an AAV vector carrying the murine *Gtf2i* cDNA (AAV9-m*Gtf2i*) under the control of the CMV promoter and containing the capsid proteins of the AAV9. As a negative control and reporter of AAV9 expression, we generated an analogous construct containing β*Gal* protein instead of m*Gtf2i* (AAV9-*βGal*). Vectors were injected into the cisterna magna in 11–12-week-old mice. One month postinjection, spread AAV9 transduction was confirmed in mice brains by immunofluorescence assays (**Supplementary Figure S3**). Additionally, *βGal* and m*Gtf2i* transduction in hippocampus was confirmed by PCR. (**Figure 3a,b and Supplementary Table S1**). *Gtf2i* mRNA levels were significantly increased (57.5%) in hippocampus from CD-m*Gtf2i*–injected mice when compared to CD-β*Gal*–injected controls (P = 0.036) or age-matched untreated CD mice (P = 0.004). As expected, AAV9-β*Gal* injection did not affect *Gtf2i* expression in neither CD nor WT mice (**Figure 3c**).

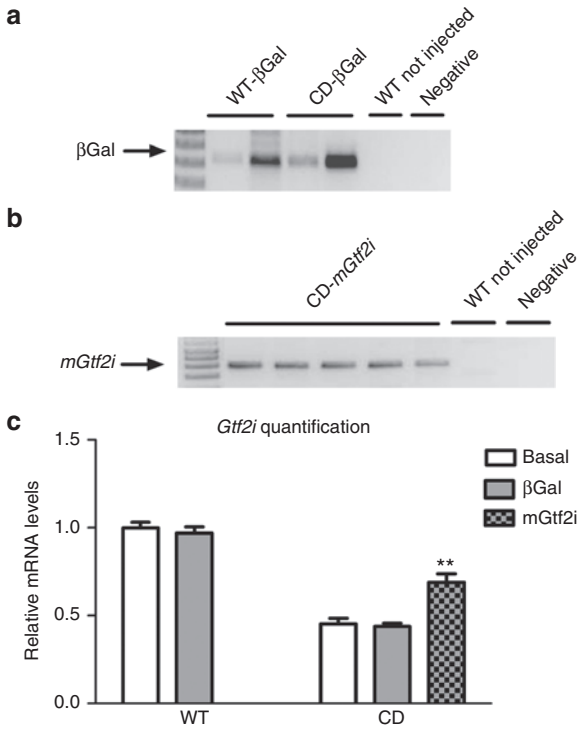

Figure 3 Efficient AAV9-mediated *Gtf2i* expression in mouse hippocampus. (**a**) One month postinjection, AAV9-*βGal* transduction was confirmed by PCR in DNA extracted from mouse brain. Lanes 1 and 2 represent two different WT mice injected with AAV9-*βGal*; lanes 3 and 4 represent two different CD mice injected with AAV9-*βGal*; lane 5 represents a noninjected WT mouse; lane 6 is the negative control of the experiment. (**b**) Presence of m*Gtf2i* transduction was confirmed by PCR in DNA extracted from mouse brain. Primers were design to span one intron to only detect ectopic m*Gtf2i*. Lanes 1 to 5 represent five different CD mice injected with AAV9-m*Gtf2i*; lane 6 represents a noninjected WT mouse; lane 7 is the negative control of the experiment. (**c**) AAV9-m*Gtf2i* intracisternal injection leads to an efficient expression of *Gtf2i* in mouse hippocampus. One month postinjection, relative *Gtf2i* mRNA levels were measured in hippocampus of CD-*βGal* and CD-m*Gtf2i*–injected mice together with untreated mice (basal). *Gtf2i* levels were increased in hippocampus from CD-m*Gtf2i* injected mice when compared to CD-*βGal* mice or age-matched untreated CD mice. Data are presented as the mean ± SEM (n = 4–18, ≥2 mice per group). P values are shown with asterisks indicating values that are significantly different in group comparisons (one-way analysis of variance followed by Bonferroni *post hoc* test). **P < 0.01.

Gtf2i ectopic expression partially improves cognitive behavior in CD mice

One month after AAV9 injection, animals were explored using the same behavioral tests as described previously.

In the social interaction test, CD-β*Gal*–injected mice showed similar behavior as CD noninjected mice with a significant increase in the time sniffing the intruder mouse (P = 0.010; **Figure 4a**). In contrast, CD-m*Gtf2i* injected mice showed less interest in the intruder mouse, behaving as WT mice (P = 0.791; **Figure 4a**).

With respect to motor coordination, all groups of mice performed better at 7 rpm, what is an expected effect due to training. However, although we could still observe significant differences between WT and CD-β*Gal*–injected mice at 10, 14, and 19 rpm ($P = 2.8 \times 10^{-5}$, P = 0.012, and P = 0.033, respectively), CD-m*Gtf2i* injected mice improved their performance in this test, not falling off the rod significantly faster than WT at any rpm (**Figure 4b**).

Concerning anxiety-like/obsessive behavior, the performance of CD-β*Gal* mice in this test was very similar to that in basal conditions ($F_{1,16}$ = 14.063; P = 0.002), while the performance of CD-m*Gtf2i* injected mice was closer to WT but still significantly different ($F_{1,20}$ = 5.915; P = 0.025; **Figure 4c**). However, at the end of the test (20 minutes), we could not appreciate any difference in the number of marbles buried between CD-m*Gtf2i*–injected mice and WT mice (P = 0.458).

Gtf2i ectopic expression partially restored synaptic plasticity markers in CD mouse hippocampus without significant effects on dendritic morphology

Although *Pik3r1* mRNA levels of CD-m*Gtf2i*–injected mice remained higher than WT ($P = 3.5 \times 10^{-7}$) and similar to the pretreated CD animals, *Bdnf* expression increased around 40% in CD mice after *Gtf2i* treatment, reaching levels similar to WT mice (P = 0.455; **Figure 5a**).

However, despite the gene expression changes after *Gtf2i* treatment, we did not observe any relevant change in the evaluated morphological parameters in the hippocampus. Dendritic length in both SR and SO was still significantly shorter (P < 0.001) in CD-m*Gtf2i*–injected mice (10–12%) when compared to the WT mice (**Figure 5b**). Spine density on apical proximal dendrites of CA1 pyramidal neurons from CD-m*Gtf2i*–injected mice was significantly reduced by 17% (P < 0.001) similar to pretreatment values (**Figure 5c**). Spine length was still reduced (7%) when compared to the WT although it was not significant (P = 0.07; **Figure 5d**).

DISCUSSION

Although significant differences in brain function and anatomy have been reported in patients with WBS, most neuropathological

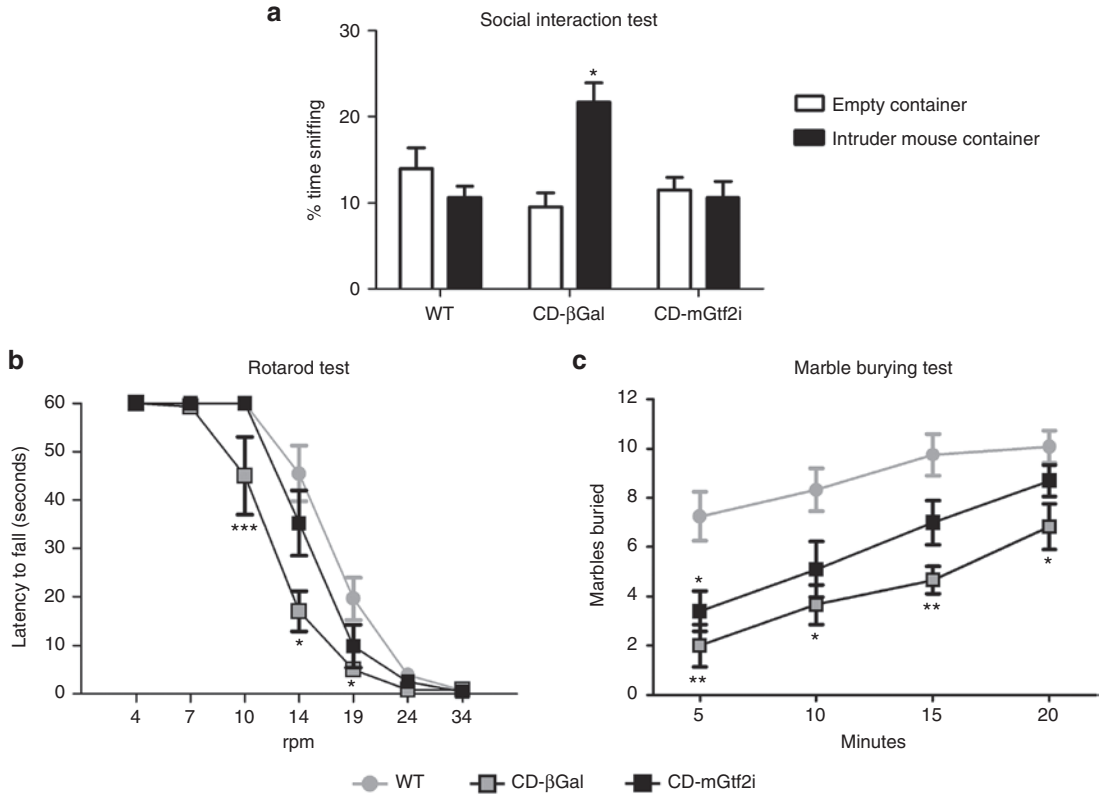

Figure 4 Cognitive behavior in CD mice after *Gtf2i* ectopic expression. (**a**) One month after injection, the interest of CD-*βGal*–injected mice in the intruder mouse was similar to the basal conditions ($P = 0.010$). However, CD-m*Gtf2i*–injected mice showed less interest in the intruder mice, behaving as WT mice ($n = 12$ WT; $n = 6$ CD-*βGal*; $n = 10$ CD-m*Gtf2i*–injected mice). (**b**) One month postinjection, CD-m*Gtf2i*–injected mice performed better in the rotarod test, not falling off the rod until 14 rpm ($P = 0.593$) as WT mice ($n = 12$ WT; $n = 6$ CD-*βGal*, $n = 10$ CD-m*Gtf2i*–injected mice). (**c**) CD-m*Gtf2i*–injected mice buried more marbles than CD-*βGal*–injected mice, although they did not reach WT values ($F_{1,20} = 5.915$; $P = 0.025$; $n = 12$ WT; $n = 6$ CD-*βGal*, $n = 10$ CD-m*Gtf2i* injected mice). Circles, WT; gray squares, CD-*βGal*; black squares, CD-m*Gtf2i*. Data are presented as the mean ± SEM. *P* values are shown with asterisks indicating values that are significantly different in individual group comparisons (general linear models of repeated measures analysis of variance or one-way analysis of variance followed by Bonferroni *post hoc* test). $*P < 0.05$; $**P < 0.01$; $***P < 0.001$.

data are limited to morphologic and volumetric differences of brain areas, and little is known about detailed cellular or dendritic abnormalities.[8,50] In addition, while there is strong evidence that *GTF2I* haploinsufficiency is a main player in most neurocognitive features of WBS,[20,28] the pathophysiologic mechanisms need to be studied in further detail.

Here, we show that hippocampal pyramidal neurons have shorter dendrites in both apical (SR) and basal (SO) compartments of CA1 hippocampus in CD, *ΔGtf2i*$^{+/-}$, and *ΔGtf2i*$^{-/-}$, although not significant in PD mice. In all mutant mice analyzed, the spines of apical dendrites of CA1 region were shorter, indicating a more immature type of spine. Additionally, *ΔGtf2i*$^{-/-}$, PD, and CD showed a reduction in spine density. It is now well established that spines are the postsynaptic sites of most excitatory synapses in the brain, receiving inputs from glutamatergic axons.[51] Shorter dendrites and decreased spine density could correlate with the reduction in the hippocampal volume and secondary dysfunction previously described in CD mice[19] (**Supplementary Figure S4a**), and also the smaller CA1 volume observed in *ΔGtf2i*$^{-/-}$ and *ΔGtf2i*$^{+/-}$ mice[20] (**Supplementary Figure S4b**). Thus, alterations in density and morphology of individual spines in WBS mouse models, critical for the regulation of synaptic excitability, suggest an abnormal development and remodeling of the connectivity of neuronal circuits in the disorder. The presence of similar phenotypes in mice with isolated or expanded *Gtf2i* hypomorphic alleles strongly indicates that GTF2I should have a relevant role in the developmental regulation of the morphology of hippocampal spines and that these hippocampal anomalies are due to its dosage deficiency.

BDNF is a neurotrophin with important roles in neuronal development and function. Decreased *BDNF* expression has been associated with mood disorders such as depression, bipolar disorder, anxiety, stress, or trauma,[52–54] and also with some neurological diseases linked to cognitive deficits including Rett and Down syndromes.[55,56] It has been hypothesized that decreased *BDNF* could be related to the smaller hippocampal volume found in patients with major depression and posttraumatic stress disorder.[57,58] We have found that *Bdnf* mRNA levels are also decreased in the hippocampus of WBS mouse models, thus probably secondary to *Gtf2i* haploinsufficiency. BDNF acts via the PI3K–Akt–mTOR and Ras–ERK signaling pathways to regulate synaptic plasticity, dendritic branching, and the number and morphology of dendritic spines.[41] Hyperactivation of the PI3K–Akt–mTOR pathway due to increased protein levels of p110 (catalytic subunit of PI3K) has been described in Fragile X syndrome.[59] We demonstrated increased levels of *Pik3r1* mRNA in the hippocampus of WBS mouse models, suggesting that the PI3K

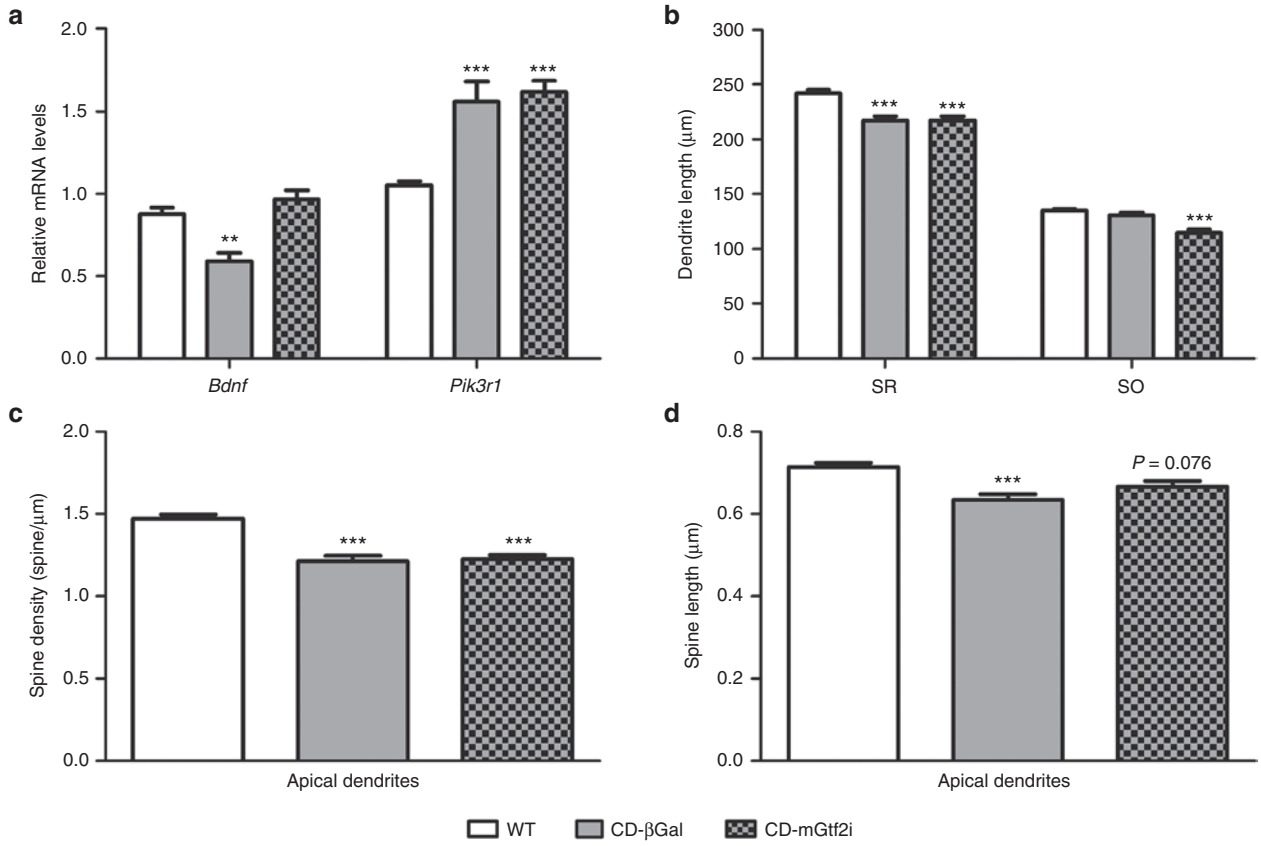

Figure 5 Neuronal architecture in CA1 pyramidal neurons and synaptic markers quantification in CD mice after *Gtf2i* ectopic expression. (**a**) One month after the treatment, *Bdnf* of CD-m*Gtf2i* mice was completely restored ($P = 0.455$). *Pik3r1* levels were still high after *Gtf2i* treatment ($P = 3.5 \times 10^{-7}$; $n = 2$–4 RT-PCRs/mice, ≥2 mice). (**b**–**d**) One month after injection, only spine length of the parameters analyzed for neuronal architecture changed in CD-m*Gtf2i* mice ($P = 0.076$). Data are presented as the mean ± SEM. *P* values are shown with asterisks indicating values that are significantly different in group comparisons (one-way analysis of variance followed by Bonferroni *post hoc* test). *$P < 0.05$; **$P < 0.01$; ***$P < 0.001$. SO, stratum oriens; SR, stratum radiatum.

signaling pathway might also be hyperactive in these mice. Since GTF2I has been shown to bind directly to the *Pi3kr1* promoter in mouse embryonic fibroblasts,[42] its effect on *Pik3r1* seems to be inhibitory as *Gtf2i* deletion leads to *Pik3r1* upregulation. These results are in line with the reported finding that *GTF2I* levels are inversely correlated with the levels of several other genes such as *BEND4*, suggesting a repressive effect of *GTF2I* on those genes.[60]

The comparative neurobehavioral phenotypic study of all four WBS mouse models in three main tasks has provided insight into the shared features or deficits most likely due to *Gtf2i* haploinsufficiency. A consistent behavioral characteristic of WBS is hypersociability, showing a social disinhibited behavior with strangers sometimes that may put themselves at risk for abuse, especially during adolescence.[25,43] In addition to our results, CD, PD, and *Gtf2i* heterozygous mice also showed altered social behavior in different paradigms of sociability.[19,21,30]

WBS individuals also show delays in the acquisition of motor skills, poor balance, and deficits in motor coordination.[4,44] Along with previous data showing that CD and PD mice had a bad performance in the rotarod,[19,21] $\Delta Gtf2i^{+/-}$ and $\Delta Gtf2i^{-/-}$ mice also showed deficits in the accelerating rotarod test as soon as 7 rpm, and $\Delta Gtf2i^{-/-}$ mice required a significantly higher number of trials to stay up in the rod at 4 rpm for 120 seconds. Finally, WBS individuals manifest high levels of anxiety, preoccupations, and/or obsessions, especially in adulthood.[4] We used the marble burying test to explore this phenotype in mice, although it is unclear whether an abnormal performance in this test reflects anxiety or obsessive-compulsive behavior.[45–47] Anyway, marble burying is believed to partially depend on hippocampal function.[48,49] CD, $\Delta Gtf2i^{-/-}$, and PD mice showed significantly reduced burying of marbles indicating hippocampal dysfunction. The discordant behavior in this test previously reported for PD mice,[21] with no differences respect to WT, could be due to methodological differences such as test protocols, housing, or feeding. Our results confirm that *Gtf2i* is a main player in the hypersociable personality as well as in the poor motor abilities and motor coordination problems of WBS. *Gtf2i* may also have an important role in anxiety-like/obsessive behavior, but other genes in the region might contribute to the phenotype, as partial loss of *Gtf2i* alone did not show differences when compared to the WT.

Finally, in order to further demonstrate the involvement of GTF2I in these phenotypes and its utility as a potential therapeutic target, we performed *in situ Gtf2i* replacement by gene therapy to rescue some of the alterations in CD mice. We used adult CD mice, harboring the almost complete deletion of the WBS locus, as the best model for the human disorder to define the phenotypic features that can be rescued by a single gene. The animals

were injected at 4 months of age, when brain development is completed. Based on reports that classify AAV9 as highly expressed and with rapid-onset kinetics,[61] we performed behavioral tests and collected samples 1 month after the injection. The efficiency was documented by a significant increase of *Gtf2i* expression (57.5%) in hippocampus of injected animals when compared to controls. CD-m*Gtf2i*–injected mice had a better performance in all the tests studied: social behavior was completely normalized; motor learning and coordination in the accelerating rotarod was nearly as good in treated CD mice as in WT mice; finally, in the marble burying test, anxiety-like behavior of CD mice was improved, although WT levels were not reached until the end of the test. These results reinforce the concept that hemizygosity of *Gtf2i* is the major cause of the overfriendly and hypersocial phenotype of WBS and an important contributor to the fine motor skills and to the anxiety phenotype. The incomplete recovery of motor skills and anxiety-like behavior may be due to several factors: (i) the bioavailability of GTF2I did not reach physiologic levels, or not in all cells relevant for the phenotype; (ii) functional recovery might be insufficient given the developmental anomalies; and (iii) additive contribution of other gene(s) in the region might be required for these phenotypes. In this regard, DD mice (deleted for distal genes not including *Gtf2i*) also showed a trend to perform worse than WT in the rotarod.[21]

Dendritic spine anomalies, likely generated due to GTF2I deficiency during developmental formation and maturation, have been identified in the hippocampus of WBS mouse models as one possible cause of altered neuronal circuitry and neurobehavioral problems. We then checked whether the phenotypic rescue by *in situ Gtf2i* gene therapy was also associated with improved plasticity of dendritic spines. Not surprisingly, the documented increase of *Gtf2i* mRNA was not enough to reverse the morphological phenotypes observed in the adult brain of CD mice. However, we hypothesized that some functional reversal must have taken place despite the absence of relevant structural changes, possibly through remodeling of already existing spines. Pharmacotherapy for Down syndrome using GABAa receptor antagonists also resulted in functional improvement with little effect on the morphological dendritic anomalies.[62] In fact, we observed a normalization of *Bdnf* expression following *Gtf2i* gene therapy, and BDNF is the main promoter of formation, maintenance, and activity-dependent sculpting of dendritic spines. Since there was no apparent effect on *Pik3r1* expression, a known target of GTF2I involved in downstream signaling of dendrites, the effect on BDNF is more likely to occur upstream and by still unknown mechanisms.

In summary, our data further reassure that *Gtf2i* deficiency is involved in the neurocognitive phenotype of WBS, causing specific neuroanatomical alterations in the hippocampus and synaptic plasticity deficits demonstrated in WBS mouse models. Increasing *Gtf2i* expression levels by gene therapy resulted in an interesting improvement of the neurocognitive phenotype of CD mice, probably through modulation of BDNF-related pathways. Although correction of morphogenesis defects might require an early treatment, appropriate replacement of GTF2I and/or BDNF deficiency in brain areas during adulthood may result in improvement of the cognitive and behavioral performance in WBS.

MATERIALS AND METHODS

Ethics statement. Animal procedures were conducted in strict accordance with the guidelines of the European Communities Directive 86/609/EEC regulating animal research and were approved by the local Committee of Ethical Animal Experimentation (CEEA-PRBB).

Animals' maintenance. WBS mutant mice (*ΔGtf2i*$^{+/-}$, *ΔGtf2i*$^{-/-}$, PD (proximal deletion; *Gtf2i-Limk1*), and CD (complete deletion; *Gtf2i-Fkbp6*)) were obtained as previously described.[19–21] WBS mutant mice were crossed with Thy1-YFP transgenic mice (B6.Cg-Tg(Thy1-YFPH)2Jrs/J, Jackson Laboratory)[63] to label pyramidal neurons.

All mice used were males and were maintained on at least 97% C57BL/6J background. Animals were housed under standard conditions in a 12 hours dark/light cycle with access to food and water ad libitum. Genomic DNA was extracted from mouse tail to determine the genotype of each mouse using multiplex ligation probe amplification and appropriate primers (**Supplementary Table S1**).

Recombinant AAV vector generation and intracisternal delivery. AAV9 recombinant adenoviruses were generated by the "Unitat de Producció de Vectors" (UPV) (CBATEG, Barcelona, Spain). The expression cassettes used were (i) *βGal* under the control of CMV promoter and SV40 polyA signal or (ii) murine cDNA *Gtf2i (*m*Gtf2i)* under the control of CMV promoter and SV40 polyA signal.

Separate groups of mice underwent intracisternal injections with 2×10^{10} vg (viral genomes) per animal of either AAV9-β*Gal* or AAV9-m*Gtf2i* at 11–12 weeks. Detailed methodology can be found in **Supplementary Materials and Methods**. We finally worked with three groups of injected animals: WT-AAV9 (n = 12), CD-β*Gal* (n = 5), and CD-m*Gtf2i* (n = 11) mice. Correct delivery of AAV9 into the brain was confirmed by immunohistofluorescence (**Supplementary Materials and Methods**).

Histological preparation. Mice were transcardially perfused with 1× PBS followed by 4% paraformaldehyde. Brains were removed and postfixed in 4% paraformaldehyde for 24 hours at 4 °C, in PBS for 24 hours at 4 °C and, afterwards, crioprotected in 30% sucrose for 24 hours at 4 °C. Finally, serial coronal sections (40 µm) of brain were collected on a glass slide and mounted with Mowiol.

Imaging. We obtained 1,024×1,024 pixel confocal fluorescent image stacks from coronal tissue sections of 40 µm using a TCS SP2 LEICA confocal microscope.

For spine quantification, an HC PL FLUOTAR ×63 (zoom 5) oil-immersion objective was used. Basal proximal (30–120 µm from soma) and apical proximal (secondary apical dendrites from 50–150 µm from soma) were selected for the analysis of spine density. The number of spines was counted using ImageJ Cell Counter plugging from 15–30 µm dendritic segments of randomly selected neurons. Spine counts included all type of dendritic protrusions. Spines located on the top or bottom surfaces of the dendrites were not counted; thus, the total number of spines was underestimated in all cases. A minimum of three animals were analyzed per genotype and 8–15 dendritic segments were analyzed per animal. Spine density was calculated by dividing the total spine count by the length of dendrite analyzed. Spine length was measured from the base of the spine neck to the end of the head of the spine.

For morphological analysis of the SR and SO, 1,360×1,024 images of CA1 hippocampus were obtained on a Leika epifluorescence microscopy at ×4 magnification. Measures from six hippocampal sections per animal (3–6 mice) were averaged.

RNA preparation and gene expression quantification. RNA was extracted from hippocampal tissues of adult mice using TRIZOL reagent (Invitrogen, Barcelona, Spain) according to the manufacturer's instructions. cDNA was prepared from 1 µg of total RNA using random hexamers

and SuperScript II RNase H reverse transcriptase (Invitrogen). The expression of *Gtf2i*, *Pik3r1*, *Bdnf*, and *Rps28* was evaluated by quantitative real-time PCR (qRT-PCR) and/or semi-quantitative RT-PCR (**Supplementary Materials and Methods**). Primers were designed to span an intron in all cases (**Supplementary Table S1**).

Behavioral tests

Social interaction test. This test was conducted in an open field. First, an empty wire cup-container was placed in the center of the arena. The subject mouse was allowed to explore the arena, and the amount of time sniffing the empty container was measured during 5 minutes. Next, an intruder mouse was hold in the container and, again, the amount of time nose to nose sniffing was measured during 5 minutes. Each animal trial was monitored and computed with a software tracking system SMART 3.0 (Panlab-Harvard Apparatus; SL, Spain) connected to a video camera placed above the arena. In parallel, two observers simultaneously scored the sniffing counts and the registered and observed results were compared subsequently.

Rotarod test. A commercially available rotarod apparatus (Rotarod LE8500; Panlab, Harvard Apparatus, Spain) was used. The experiment consisted of two trials: training criterion test, in which animals were trained until they could stay on the rod at the minimum speed (4 rpm) during 120 seconds; and the test session, in which motor coordination and motor skill learning were evaluated by measuring the latency to fall off the rod in consecutive trials of 4, 10, 14, 19, 24, and 34 rpm. Animals were allowed to stay on the rod for a maximum period of 60 seconds per trial and to rest between trials during 5 minutes.

Marble burying test. The test was conducted in a polycarbonate rat cage filled with bedding to a depth of 5 cm and lightly tamped down. A regular pattern of 20 glass marbles (five rows of four marbles) were placed on the surface of the bedding prior to each test. An individual animal was placed in each cage. The number of buried marbles (>2/3 marble covered) was counted every 5 minutes during 20 minutes.

In all experiments, investigators were blinded to genotypes and to treatment.

Statistical analyses. Results are presented as mean ± SEM. All data were analyzed using a one-way analysis of variance followed by Bonferroni *post-hoc* test when there were more than two groups or a nonparametric Mann–Whitney *U*-test for two groups. A General Linear Models of repeated measures analysis of variance was used in the analysis of marble burying test. All statistical tests were made under the SPSS environment. Values of $P < 0.05$ were considered significant.

SUPPLEMENTARY MATERIAL

Figure S1. Basal and apical proximal dendritic spine morphology in CA1 pyramidal neurons.

Figure S2. Learning the rotarod test at 4 rpm in $\Delta Gtf2i^{-/-}$ mice.

Figure S3. Immunohistofluorescence assay confirming AAV9 transduction in the brain.

Figure S4. CA1 area volumes in $\Delta Gtf2i^{+/-}$, $\Delta Gtf2i^{-/-}$, and CD mice.

Table S1. Primer sequences for genotyping and expression experiments.

Materials and Methods

ACKNOWLEDGMENTS

This work was supported by the Spanish Ministry of Economy and Competitivity (grant SAF2012-40036 to V.C.) and the Catalan Government (2009SGR1274, 2014SGR1468, and ICREA Acadèmia to L.A.P.-J.), The CIBER for Rare Diseases (CIBERER) and AGAUR fellowships supported C.B. The authors gratefully acknowledge Fernando J. Pérez-Asensio, Laura Espanya, and Ana Rodríguez for technical assistance with mouse handling.

The work is a product of the intellectual environment of the whole team; and all members have contributed in various degrees to the analytical methods used, to the research concept, and to the experiment design. No author has financial interests relative to this manuscript.

REFERENCES

1. Pérez Jurado, AL (2003). Williams-Beuren syndrome: a model of recurrent genomic mutation. *Horm Res* **59** (suppl. 1): 106–113.
2. Bayés, M, Magano, LF, Rivera, N, Flores, R and Pérez Jurado, LA (2003). Mutational mechanisms of Williams-Beuren syndrome deletions. *Am J Hum Genet* **73**: 131–151.
3. Strømme, P, Bjørnstad, PG and Ramstad, K (2002). Prevalence estimation of Williams syndrome. *J Child Neurol* **17**: 269–271.
4. Pober, BR (2010). Williams-Beuren syndrome. *N Engl J Med* **362**: 239–252.
5. Morris, CA (2010). The behavioral phenotype of Williams syndrome: a recognizable pattern of neurodevelopment. *Am J Med Genet C Semin Med Genet* **154C**: 427–431.
6. Chiang, MC, Reiss, AL, Lee, AD, Bellugi, U, Galaburda, AM, Korenberg, JR *et al.* (2007). 3D pattern of brain abnormalities in Williams syndrome visualized using tensor-based morphometry. *Neuroimage* **36**: 1096–1109.
7. Reiss, AL, Eliez, S, Schmitt, JE, Straus, E, Lai, Z, Jones, W *et al.* (2000). IV. Neuroanatomy of Williams syndrome: a high-resolution MRI study. *J Cogn Neurosci* **12** (suppl. 1): 65–73.
8. Reiss, AL, Eckert, MA, Rose, FE, Karchemskiy, A, Kesler, S, Chang, M *et al.* (2004). An experiment of nature: brain anatomy parallels cognition and behavior in Williams syndrome. *J Neurosci* **24**: 5009–5015.
9. Thompson, PM, Lee, AD, Dutton, RA, Geaga, JA, Hayashi, KM, Eckert, MA *et al.* (2005). Abnormal cortical complexity and thickness profiles mapped in Williams syndrome. *J Neurosci* **25**: 4146–4158.
10. Faria, AV, Landau, B, O'Hearn, KM, Li, X, Jiang, H, Oishi, K *et al.* (2012). Quantitative analysis of gray and white matter in Williams syndrome. *Neuroreport* **23**: 283–289.
11. Meyer-Lindenberg, A, Mervis, CB, Sarpal, D, Koch, P, Steele, S, Kohn, P *et al.* (2005). Functional, structural, and metabolic abnormalities of the hippocampal formation in Williams syndrome. *J Clin Invest* **115**: 1888–1895.
12. Tomaiuolo, F, Di Paola, M, Caravale, B, Vicari, S, Petrides, M and Caltagirone, C (2002). Morphology and morphometry of the corpus callosum in Williams syndrome: a T1-weighted MRI study. *Neuroreport* **13**: 2281–2284.
13. Schmitt, JE, Eliez, S, Bellugi, U and Reiss, AL (2001). Analysis of cerebral shape in Williams syndrome. *Arch Neurol* **58**: 283–287.
14. Gaser, C, Luders, E, Thompson, PM, Lee, AD, Dutton, RA, Geaga, JA *et al.* (2006). Increased local gyrification mapped in Williams syndrome. *Neuroimage* **33**: 46–54.
15. Van Essen, DC, Dierker, D, Snyder, AZ, Raichle, ME, Reiss, AL and Korenberg, J (2006). Symmetry of cortical folding abnormalities in Williams syndrome revealed by surface-based analyses. *J Neurosci* **26**: 5470–5483.
16. Mobbs, D, Eckert, MA, Menon, V, Mills, D, Korenberg, J, Galaburda, AM *et al.* (2007). Reduced parietal and visual cortical activation during global processing in Williams syndrome. *Dev Med Child Neurol* **49**: 433–438.
17. Jackowski, AP, Rando, K, Maria de Araújo, C, Del Cole, CG, Silva, I and Tavares de Lacerda, AL (2009). Brain abnormalities in Williams syndrome: a review of structural and functional magnetic resonance imaging findings. *Eur J Paediatr Neurol* **13**: 305–316.
18. Binelli, C, Subirà, S, Batalla, A, Muñiz, A, Sugranyés, G, Crippa, JA *et al.* (2014). Common and distinct neural correlates of facial emotion processing in social anxiety disorder and Williams syndrome: a systematic review and voxel-based meta-analysis of functional resonance imaging studies. *Neuropsychologia* (epub ahead of print).
19. Segura-Puimedon, M, Sahún, I, Velot, E, Dubus, P, Borralleras, C, Rodrigues, AJ *et al.* (2014). Heterozygous deletion of the Williams-Beuren syndrome critical interval in mice recapitulates most features of the human disorder. *Hum Mol Genet* **23**: 6481–6494.
20. Lucena, J, Pezzi, S, Aso, E, Valero, MC, Carreiro, C, Dubus, P *et al.* (2010). Essential role of the N-terminal region of TFII-I in viability and behavior. *BMC Med Genet* **11**: 61.
21. Li, HH, Roy, M, Kuscuoglu, U, Spencer, CM, Halm, B, Harrison, KC *et al.* (2009). Induced chromosome deletions cause hypersociability and other features of Williams-Beuren syndrome in mice. *EMBO Mol Med* **1**: 50–65.
22. Zhao, C, Avilés, C, Abel, RA, Almli, CR, McQuillen, P and Pleasure, SJ (2005). Hippocampal and visuospatial learning defects in mice with a deletion of frizzled 9, a gene in the Williams syndrome deletion interval. *Development* **132**: 2917–2927.
23. van Hagen, JM, van der Geest, JN, van der Giessen, RS, Lagers-van Haselen, GC, Eussen, HJ, Gille, JJ *et al.* (2007). Contribution of CYLN2 and GTF2IRD1 to neurological and cognitive symptoms in Williams Syndrome. *Neurobiol Dis* **26**: 112–124.
24. Capossela, S, Muzio, L, Bertolo, A, Bianchi, V, Dati, G, Chaabane, L *et al.* (2012). Growth defects and impaired cognitive-behavioral abilities in mice with knockout for Eif4h, a gene located in the mouse homolog of the Williams-Beuren syndrome critical region. *Am J Pathol* **180**: 1121–1135.
25. Dai, L, Bellugi, U, Chen, XN, Pulst-Korenberg, AM, Järvinen-Pasley, A, Tirosh-Wagner, T *et al.* (2009). Is it Williams syndrome? GTF2IRD1 implicated in visual-spatial construction and GTF2I in sociability revealed by high resolution arrays. *Am J Med Genet A* **149A**: 302–314.
26. Howald, C, Merla, G, Digilio, MC, Amenta, S, Lyle, R, Deutsch, S *et al.* (2006). Two high throughput technologies to detect segmental aneuploidies identify new Williams-Beuren syndrome patients with atypical deletions. *J Med Genet* **43**: 266–273.
27. Järvinen-Pasley, A, Bellugi, U, Reilly, J, Mills, DL, Galaburda, A, Reiss, AL *et al.* (2008). Defining the social phenotype in Williams syndrome: a model for linking gene, the brain, and behavior. *Dev Psychopathol* **20**: 1–35.
28. Antonell, A, Del Campo, M, Magano, LF, Kaufmann, L, de la Iglesia, JM, Gallastegui, F *et al.* (2010). Partial 7q11.23 deletions further implicate GTF2I and GTF2IRD1 as the main genes responsible for the Williams-Beuren syndrome neurocognitive profile. *J Med Genet* **47**: 312–320.
29. Edelmann, L, Prosnitz, A, Pardo, S, Bhatt, J, Cohen, N, Lauriat, T *et al.* (2007). An atypical deletion of the Williams-Beuren syndrome interval implicates genes associated with defective visuospatial processing and autism. *J Med Genet* **44**: 136–143.
30. Sakurai, T, Dorr, NP, Takahashi, N, McInnes, LA, Elder, GA and Buxbaum, JD (2011). Haploinsufficiency of Gtf2i, a gene deleted in Williams Syndrome, leads to increases in social interactions. *Autism Res* **4**: 28–39.
31. Daya, S and Berns, KI (2008). Gene therapy using adeno-associated virus vectors. *Clin Microbiol Rev* **21**: 583–593.

32. Büning, H, Perabo, L, Coutelle, O, Quadt-Humme, S and Hallek, M (2008). Recent developments in adeno-associated virus vector technology. *J Gene Med* **10**: 717–733.
33. Niemeyer, GP, Herzog, RW, Mount, J, Arruda, VR, Tillson, DM, Hathcock, J *et al.* (2009). Long-term correction of inhibitor-prone hemophilia B dogs treated with liver-directed AAV2-mediated factor IX gene therapy. *Blood* **113**: 797–806.
34. Jiang, H, Lillicrap, D, Patarroyo-White, S, Liu, T, Qian, X, Scallan, CD *et al.* (2006). Multiyear therapeutic benefit of AAV serotypes 2, 6, and 8 delivering factor VIII to hemophilia A mice and dogs. *Blood* **108**: 107–115.
35. Ernfors, P, Lee, KF and Jaenisch, R (1994). Mice lacking brain-derived neurotrophic factor develop with sensory deficits. *Nature* **368**: 147–150.
36. Korte, M, Carroll, P, Wolf, E, Brem, G, Thoenen, H and Bonhoeffer, T (1995). Hippocampal long-term potentiation is impaired in mice lacking brain-derived neurotrophic factor. *Proc Natl Acad Sci USA* **92**: 8856–8860.
37. Hall, J, Thomas, KL and Everitt, BJ (2000). Rapid and selective induction of BDNF expression in the hippocampus during contextual learning. *Nat Neurosci* **3**: 533–535.
38. Linnarsson, S, Björklund, A and Ernfors, P (1997). Learning deficit in BDNF mutant mice. *Eur J Neurosci* **9**: 2581–2587.
39. Bramham, CR and Wells, DG (2007). Dendritic mRNA: transport, translation and function. *Nat Rev Neurosci* **8**: 776–789.
40. Santos, AR, Comprido, D and Duarte, CB (2010). Regulation of local translation at the synapse by BDNF. *Prog Neurobiol* **92**: 505–516.
41. Kumar, V, Zhang, MX, Swank, MW, Kunz, J and Wu, GY (2005). Regulation of dendritic morphogenesis by Ras-PI3K-Akt-mTOR and Ras-MAPK signaling pathways. *J Neurosci* **25**: 11288–11299.
42. Segura-Puimedon, M, Borralleras, C, Pérez-Jurado, LA and Campuzano, V (2013). TFII-I regulates target genes in the PI-3K and TGF-β signaling pathways through a novel DNA binding motif. *Gene* **527**: 529–536.
43. Doyle, TF, Bellugi, U, Korenberg, JR and Graham, J (2004). "Everybody in the world is my friend" hypersociability in young children with Williams syndrome. *Am J Med Genet A* **124A**: 263–273.
44. Gagliardi, C, Martelli, S, Burt, MD and Borgatti, R (2007). Evolution of neurologic features in Williams syndrome. *Pediatr Neurol* **36**: 301–306.
45. Thomas, A, Burant, A, Bui, N, Graham, D, Yuva-Paylor, LA and Paylor, R (2009). Marble burying reflects a repetitive and perseverative behavior more than novelty-induced anxiety. *Psychopharmacology (Berl)* **204**: 361–373.
46. Takeuchi, H, Yatsugi, S and Yamaguchi, T (2002). Effect of YM992, a novel antidepressant with selective serotonin re-uptake inhibitory and 5-HT 2A receptor antagonistic activity, on a marble-burying behavior test as an obsessive-compulsive disorder model. *Jpn J Pharmacol* **90**: 197–200.
47. Njung'e, K and Handley, SL (1991). Evaluation of marble-burying behavior as a model of anxiety. *Pharmacol Biochem Behav* **38**: 63–67.
48. Deacon, RM and Rawlins, JN (2005). Hippocampal lesions, species-typical behaviours and anxiety in mice. *Behav Brain Res* **156**: 241–249.
49. Deacon, RM (2006). Digging and marble burying in mice: simple methods for *in vivo* identification of biological impacts. *Nat Protoc* **1**: 122–124.
50. Meyer-Lindenberg, A, Mervis, CB and Berman, KF (2006). Neural mechanisms in Williams syndrome: a unique window to genetic influences on cognition and behaviour. *Nat Rev Neurosci* **7**: 380–393.
51. Sala, C and Segal, M (2014). Dendritic spines: the locus of structural and functional plasticity. *Physiol Rev* **94**: 141–188.
52. Duman, RS and Monteggia, LM (2006). A neurotrophic model for stress-related mood disorders. *Biol Psychiatry* **59**: 1116–1127.
53. Monteggia, LM, Barrot, M, Powell, CM, Berton, O, Galanis, V, Gemelli, T *et al.* (2004). Essential role of brain-derived neurotrophic factor in adult hippocampal function. *Proc Natl Acad Sci USA* **101**: 10827–10832.
54. Kapczinski, F, Frey, BN, Kauer-Sant'Anna, M and Grassi-Oliveira, R (2008). Brain-derived neurotrophic factor and neuroplasticity in bipolar disorder. *Expert Rev Neurother* **8**: 1101–1113.
55. Sun, YE and Wu, H (2006). The ups and downs of BDNF in Rett syndrome. *Neuron* **49**: 321–323.
56. Tlili, A, Hoischen, A, Ripoll, C, Benabou, E, Badel, A, Ronan, A *et al.* (2012). BDNF and DYRK1A are variable and inversely correlated in lymphoblastoid cell lines from Down syndrome patients. *Mol Neurobiol* **46**: 297–303.
57. Bremner, JD, Narayan, M, Anderson, ER, Staib, LH, Miller, HL and Charney, DS (2000). Hippocampal volume reduction in major depression. *Am J Psychiatry* **157**: 115–118.
58. Bremner, JD (2002). Neuroimaging studies in post-traumatic stress disorder. *Curr Psychiatry Rep* **4**: 254–263.
59. Sharma, A, Hoeffer, CA, Takayasu, Y, Miyawaki, T, McBride, SM, Klann, E *et al.* (2010). Dysregulation of mTOR signaling in fragile X syndrome. *J Neurosci* **30**: 694–702.
60. Adamo, A, Atashpaz, S, Germain, PL, Zanella, M, D'Agostino, G, Albertin, V *et al.* (2015). 7q11.23 dosage-dependent dysregulation in human pluripotent stem cells affects transcriptional programs in disease-relevant lineages. *Nat Genet* **47**: 132–141.
61. Zincarelli, C, Soltys, S, Rengo, G and Rabinowitz, JE (2008). Analysis of AAV serotypes 1-9 mediated gene expression and tropism in mice after systemic injection. *Mol Ther* **16**: 1073–1080.
62. Fernandez, F, Morishita, W, Zuniga, E, Nguyen, J, Blank, M, Malenka, RC *et al.* (2007). Pharmacotherapy for cognitive impairment in a mouse model of Down syndrome. *Nat Neurosci* **10**: 411–413.
63. Feng, G, Mellor, RH, Bernstein, M, Keller-Peck, C, Nguyen, QT, Wallace, M *et al.* (2000). Imaging neuronal subsets in transgenic mice expressing multiple spectral variants of GFP. *Neuron* **28**: 41–51.